Accuracy of Eigenvalue Derivatives from Reduced-Order Structural Models

Chris A. Sandridge* and Raphael T. Haftka†
Virginia Polytechnic Institute and State University, Blacksburg, Virginia

It is well known that the Fourier series of discontinuous functions converge slowly and that the derivatives of the series may not converge at all. Since modal expansion of structural response is a generalization of the Fourier series, we may expect slow convergence of modal expansion when the applied loads exhibit discontinuities in time or space. Thus, in a structure controlled by point actuators, we may expect slow convergence of derivatives of structural response with respect to system parameters. To demonstrate this, the sensitivity of the closed-loop response to structural changes is calculated for a multispan beam with direct-rate feedback using colocated velocity sensors and point actuators. Reduced models based on the natural modes of the structure are formed, and derivatives of the damping ratios of the closed-loop eigenvalues are calculated. As expected, the convergence of the derivatives of the damping ratios with an increasing number of modes is slower than the convergence of the damping ratios themselves. The convergence is improved when distributed actuators replace the point actuators. In transient response problems, it is known that complementing the vibration modes with a mode representing static response to the loads can improve convergence. Indeed, for the example studied, when Ritz vectors corresponding to static responses caused by unit loads at the actuators are added to the basis vectors, the convergence of the reduced-model derivatives is greatly enhanced.

Introduction

BECAUSE large space structures are flexible and have little inherent damping, active control systems are needed to damp out vibrations. A full finite-element model of a space structure may have thousands of degrees of freedom and is not practical for use with most control system design algorithms. Therefore, a reduced model based on a small number of natural vibration modes is commonly used to design the control system.

The errors associated with the reduced model can cause the control system to become unstable. For example, spillover instability[1] is associated with the excitation of higher-order modes that are not included in the reduced model. However, it is usually possible to overcome these instabilities by special techniques[2] or by building enough robustness into the control design.

Recently, there has been interest in designing the control system and the structure simultaneously.[3] This is based on indications that small changes in the structure can significantly reduce the control effort needed to damp vibrations, thus lowering the total cost of the structure and control.[4] For such combined optimization, the sensitivity of the control system to changes in the structure is needed and errors in the derivatives associated with model reduction become a serious concern.

It has been shown that the convergence of the derivatives of the structural response with increasing number of modes can be much slower than the convergence of the response itself.[5,6] The problem of slow modal convergence of derivatives can be expected to be more severe for large space structures, which typically have a large number of closely spaced frequencies.

Modal expansion is a generalization of the Fourier series. It is well known that the Fourier series of discontinuous functions converge slowly and that the derivatives of the series may not converge at all. Accordingly, we may expect slow convergence of modal expansion when the applied loads exhibit discontinuities in time or space. This was demonstrated for the transient response of a string under a point load.[5] In a controlled structure, where most of the damping is supplied by the control system, convergence problems may be caused by point actuators. The purpose of the present paper is to demonstrate that such convergence problems can also be encountered for the eigenvalues of the controlled system and to suggest a possible remedy. This is done by calculating the derivatives of damping ratios with respect to structural changes for a flexible, multispan beam controlled by two point actuators.

Convergence of Fourier Series and Derivative of a Step Function

Consider a step function

$$f(x)=\begin{cases}0 & -l<x<0\\ p & 0<x<l\end{cases} \tag{1}$$

The Fourier series for the function is

$$f(x)=\frac{p}{2}+\frac{2p}{\pi}\sum_{m=1}^{\infty}\left(\frac{1}{2m-1}\right)\sin\left[\frac{(2m-1)\pi x}{l}\right] \tag{2}$$

The derivative with respect to the length of the interval l is

$$\frac{\partial f}{\partial l}=-\frac{2px}{l^2}\sum_{m=1}^{\infty}\cos\left[\frac{(2m-1)\pi x}{l}\right] \tag{3}$$

We chose the derivative with respect to l because it changes the basis functions of the series much like a change in a structure would change the mode shapes in a modal analysis. Figure 1 shows the convergence of the series and its derivative for $p=0.75$ at $x=l/10$ [the exact values are $f(l/10)=0.75$ and $(\partial f/\partial l)(l/10)=0$]. The figure shows that, even though the function converges fairly quickly, the derivative never converges. This demonstrates that sines and cosines are not good basis functions for describing the derivative of a step function.

Presented as Paper 87-0905 at the AIAA Dynamics Specialist Conference, Monterey, CA, April 9–10, 1987; received Aug. 20, 1987; revision received June 13, 1988. This paper is declared a work of the U.S. Government and is not subject to copyright protection in the United States.

*Graduate Assistant, Department of Aerospace and Ocean Engineering.

†Professor, Department of Aerospace and Ocean Engineering.

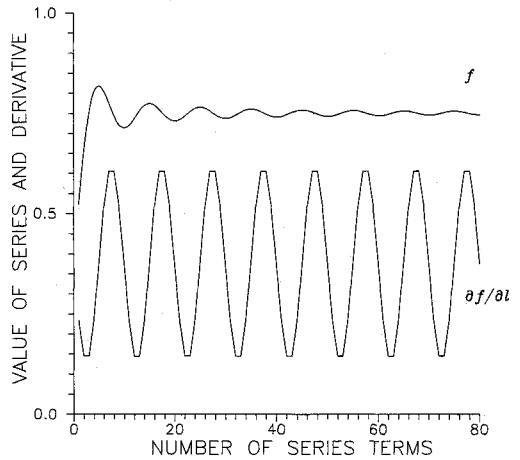

Fig. 1 Convergence of Fourier series of a step function and its derivative.

Similarly, we will show that mode shapes are not a good set of basis functions for calculating the derivative of closed-loop eigenvalues when point actuators are used.

Eigenvalue Derivative Calculation

Finite-Element Formulation

The equations of motion for an n degree-of-freedom structure with direct-rate feedback control producted by velocity sensors and force actuators are

$$M\ddot{U} + C\dot{U} + KU = 0 \tag{4}$$

where M, C, and K are the mass, damping, and stiffness matrices, respectively, and U is the structural response vector. For colocated velocity sensors and force actuator pairs, C has nonzero entries (c_i) on the diagonal corresponding to the location of the sensor-actuator pair. The value of c_i depends on the magnitude of the control grain. Assuming a solution of the form

$$U(t) = U_0 e^{\lambda_r t} \tag{5}$$

the associated eigenvalue problem is

$$(\lambda_r^2 M + \lambda_r C + K)U_r = 0 \tag{6}$$

The solution of Eq. (6) yields $2n$ real and complex eigenvalues:

$$\lambda_r = \sigma_r + i\omega_r, \qquad r = 1,...,2n \tag{7}$$

where σ_r and ω_r are real and imaginary parts of the eigenvalues. For the lightly damped system discussed in the present paper, the eigenvalues are complex conjugate pairs.

The damping ratio (ζ_r) is defined as

$$\zeta_r = -\sigma_r/(\sigma_r^2 + \omega_r^2)^{\frac{1}{2}} \tag{8}$$

The damping ratio is a measure of the effectiveness of the control for a particular mode and is used here to represent the control system performance.

To find the derivative of ζ_r with respect to a structural parameter x_i, we need the derivative of the eigenvalue. Differentiating Eq. (6) with respect to x_i, we get

$$(\lambda_r^2 M + \lambda_r C + K)\frac{\partial U_r}{\partial x_i} + \left(2\lambda_r \frac{\partial \lambda_r}{\partial x_i} M + \lambda_r^2 \frac{\partial M}{\partial x_i} + \frac{\partial \lambda_r}{\partial x_i} C + \lambda_r \frac{\partial C}{\partial x_i} + \frac{\partial K}{\partial x_i}\right) U_r = 0 \tag{9}$$

By premultiplying Eq. (9) by U_r^T and simplifying, we get

$$\frac{\partial \lambda_r}{\partial x_i} = -\frac{\lambda_r^2 U_r^T \frac{\partial M}{\partial x_i} U_r + \lambda_r U_r^T \frac{\partial C}{\partial x_i} U_r + U_r^T \frac{\partial K}{\partial x_i} U_r}{2\lambda_r U_r^T M U_r + U_r^T C U_r} \tag{10}$$

Equation (10) can be expressed as

$$\frac{\partial \lambda_r}{\partial x_i} = \frac{\partial \sigma_r}{\partial x_i} \pm i\frac{\partial \omega_r}{\partial x_i} \tag{11}$$

The derivative of the damping ratio can now be calculated by differentiating Eq. (8) to get

$$\frac{\partial \zeta_r}{\partial x_i} = \frac{\omega_r\left(\sigma_r \frac{\partial \omega_r}{\partial x_i} - \omega_r \frac{\partial \sigma_r}{\partial x_i}\right)}{(\sigma_r^2 + \omega_r^2)^{\frac{3}{2}}} \tag{12}$$

To calculate the derivative of the damping ratio with the full finite-element model, we first solve Eq. (6) for the eigenvalues and eigenvectors. We then calculate the derivative of the mass, stiffness, and damping matrices either by finite differences or analytically. Next, we calculate the derivative of the eigenvalue using Eq. (10) and, finally, we calculate the derivative of the damping ratio from Eq. (12). The derivative obtained by this process is denoted the "full-finite-element" derivative.

Reduced-Model Formulation

We now assume the displacement can be approximated as a linear combination of N modes

$$U_0 = \sum_{i=1}^{N} \phi_i v_i, \qquad N < n \tag{13}$$

where ϕ_i is the ith mode shape and v_i is the modal amplitude. The reduced eigenvalue problem corresponding to the modal coordinates is

$$(\lambda_r^2 \hat{M} + \lambda_r \hat{C} + \hat{K})V_r = 0 \tag{14}$$

where V_r is the rth reduced-model eigenvector and

$$\hat{M} = \Phi^T M \Phi, \qquad \hat{C} = \Phi^T C \Phi, \qquad \hat{K} = \Phi^T K \Phi \tag{15}$$

where Φ is a matrix with columns corresponding to the N modes used in the reduced model. When natural vibration modes are used, $\hat{M}$ and $\hat{K}$ are diagonal matrices, but for point actuators, $\hat{C}$, in general, is not diagonal.

There are several ways to calculate the derivatives of the damping ratios obtained from the reduced model. The first is to approximate U_r in terms of V_r using Eq. (13) and then use Eqs. (10) and (12) as before. A second approach is to proceed as in Eqs. (9–12), replacing M, C, K and U_r with $\hat{M}$, $\hat{C}$, $\hat{K}$, and V_r, respectively. The derivatives of $\hat{M}$, $\hat{C}$, and $\hat{K}$ can be obtained in terms of the derivatives of M, C, K, and Φ. For instance, $\partial \hat{M}/\partial x_i$ is given as

$$\frac{\partial \hat{M}}{\partial x_i} = \frac{\partial}{\partial x_i}(\Phi^T M \Phi) = 2\frac{\partial \Phi^T}{\partial x_i}(M\Phi) + \Phi^T \frac{\partial M}{\partial x_i}\Phi \tag{16}$$

If the modes used in Eq. (13) are fixed as the structure changes, the first term in Eq. (16) is zero, and we get the same approximation as with the first approach above. This approximation is denoted here the "fixed-mode" derivative.

If the modes depend on the structure (as is the case with natural vibration modes), Eq. (16) requires the derivatives of the modes. Since this reduced-model derivative reflects the updating of the modes, it will be called the "updated-mode" derivative.

In the present work, the natural vibration modes of the structure are used to reduce the model. To avoid calculating

derivatives of the updated modes in Eq. (16), $\partial\zeta_r/\partial x_i$ is calculated by finite differences. That is, the design variable x_i is perturbed, new modes are calculated, a new reduced model is formed, and ζ_r is recalculated.

Multispan Beam Example

To simulate a flexible space structure, a multispan, flexible beam (Fig. 2) was chosen because its frequencies are closely spaced. A closed-form, continuum solution (Ref. 7 and the Appendix) is available for mode shapes and frequencies. However, since the formulation involves hyperbolic sine and cosine functions, quadruple numerical precision (128-bit floating-point precision) was needed to calculate the higher modes and, even then, only 60 modes could be calculated accurately.

The five-span beam was also modeled with beam finite elements using Engineering Analysis Language (EAL), a general purpose, finite-element, structural-analysis program.[8] EAL is composed of processors that perform calculations such as model formulation, stress analysis, and dynamic response. It is possible to add user-written processors that have access to the program data base. Most of the derivative calculations in this work were performed using EAL processors.

Several finite-element models of the beam were analyzed ranging from 3 elements per span (15 elements total) to 12 elements per span (60 elements total). Table 1 shows the first 10 natural frequencies obtained from the continuum solution and from the three finite-element solutions.

Two massless controllers were placed on the beam as shown in Fig. 2; the first was a displacement-rate controller on the second span, and the second was a rotation-rate controller on the middle span. The controllers, which consist of a force actuator colocated with a velocity sensor, act as viscous dampers with damping constants c_1 and c_2 and were designed to produce damping ratios between 1 and 10% for the first 10 modes.

Table 2 shows the damping ratios of the first 10 modes for the three finite-element models, with $c_1 = 0.008$ lb · s · in.$^{-1}$ and $c_2 = 1.2$ lb · in · s. From Tables 1 and 2 it is clear that even the coarsest model is quite accurate for the first six frequencies and damping ratios.

The structural design variable used in the sensitivity analysis is the addition of a concentrated mass at points A or B on the beam (see Fig. 2). We first considered the addition of mass at point A. First, the damping ratio ζ_r and the derivatives of the damping ratio with respect to a concentrated mass $(\partial\zeta_r/\partial m)$ were calculated analytically using the full finite-element model. Then the vibration modes were calculated for the finite-element model, and reduced-model derivatives of the damping ratios were computed for increasing number of modes (up to a number of modes equal to the number of unrestrained degrees of freedom in the finite-element model). The fixed-mode derivatives were calculated analytically. The updated-mode derivatives were calculated by central finite differences as

$$\frac{\partial\zeta_r}{\partial m} \cong \frac{\zeta_r(\Delta m) - \zeta_r(-\Delta m)}{2\Delta m} \tag{17}$$

Figure 3 shows the value of $(\partial\zeta_1/\partial m)$ as a function of the step size (Δm) using 15 modes and the 15-element model. For small values of Δm, accuracy is poor due to roundoff errors, whereas for large values of Δm, the truncation error is excessive. A step size of 5×10^{-7} lb · s^2 · in.$^{-1}$ was selected.

Error of Derivative of Damping Ratio

Coarse Finite-Element Model

The first set of results were obtained for the 15-element model, which has 26 unrestrained degrees of freedom. The first six damping ratios for this model have errors of <1.5%

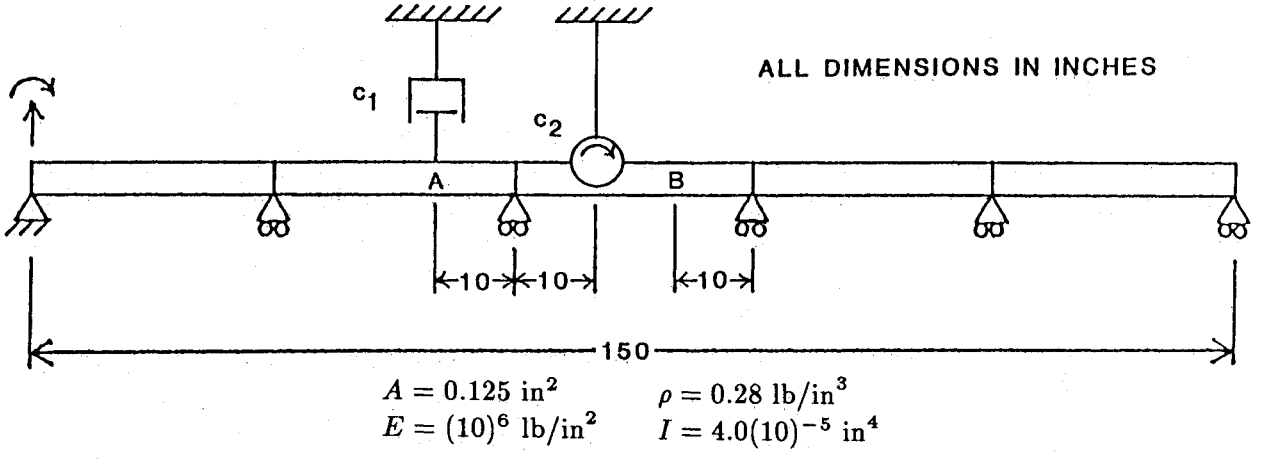

Fig. 2 Multispan beam geometry.

Table 1 Natural frequencies (Hz) of multispan beam

Mode	Continuum model	Finite element models		
		15-element	30-element	60-element
1	1.159223	1.160160	1.159281	1.159227
2	1.286099	1.287377	1.286179	1.286104
3	1.608256	1.610749	1.608414	1.608264
4	2.025720	2.030678	2.026035	2.025737
5	2.432052	2.440590	2.432600	2.432082
6	4.636892	4.691668	4.640615	4.637102
7	4.901461	4.965402	4.905860	4.901711
8	5.508898	5.596371	5.515144	5.509262
9	6.239599	6.357656	6.248659	6.240135
10	6.922233	7.063390	6.934594	6.922976

Table 2 Damping ratios of first 10 modes

Mode	15-element	30-element	60-element
1	0.0907109	0.0904736	0.0904462
2	0.0255612	0.0255043	0.0254988
3	0.0778104	0.0774696	0.0774506
4	0.0574582	0.0571145	0.0570915
5	0.0955770	0.0947231	0.0946659
6	0.0145501	0.0143603	0.0143460
7	0.0312876	0.0300424	0.0299601
8	0.0145351	0.0142391	0.0142142
9	0.0392655	0.0376863	0.0375407
10	0.0195291	0.0188517	0.0187872

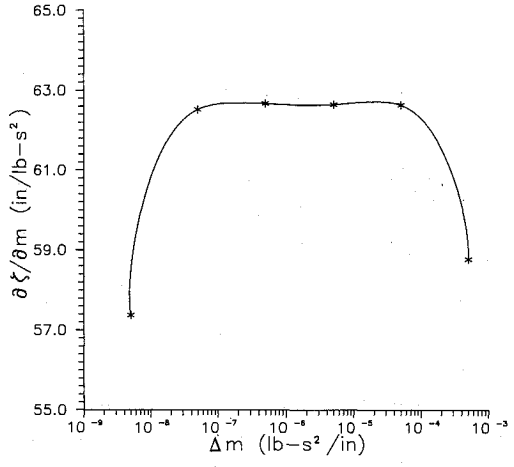

Fig. 3 Derivative of first damping ratio vs finite-difference step size.

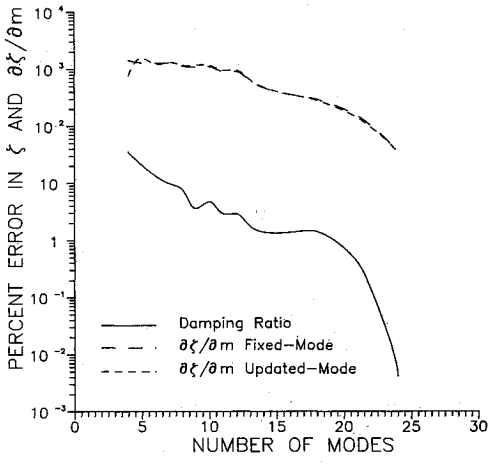

Fig. 5 Convergence of mode 4 damping ratio and derivative.

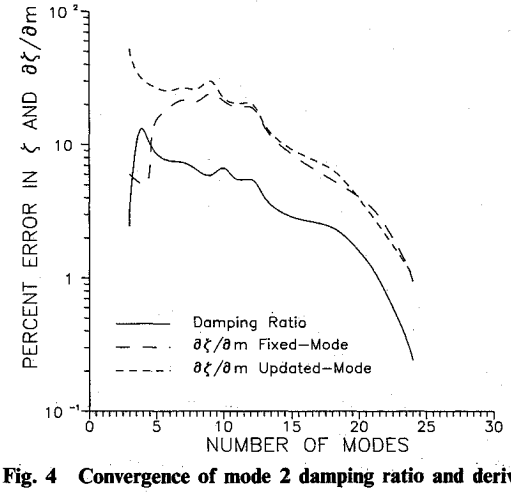

Fig. 4 Convergence of mode 2 damping ratio and derivative.

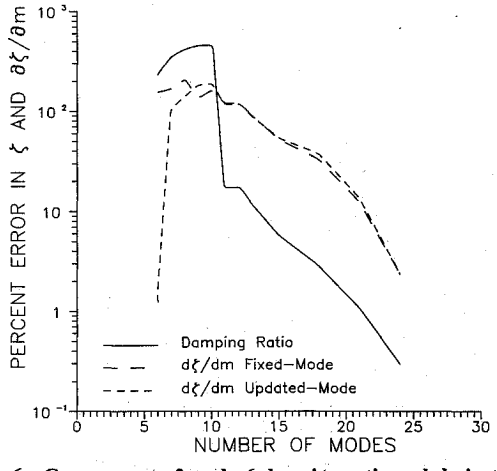

Fig. 6 Convergence of mode 6 damping ratio and derivative.

(with respect to the 30-element model), whereas the seventh damping ratio has an error of >4%. Therefore, derivatives of the first six damping ratios with respect to the added mass were calculated using the finite-element model without any modal approximation (see Table 3).

Next, damping ratios and their derivatives based on reduced models with up to 24 models were calculated. Errors in the damping ratios and their derivatives were calculated with respect to the full-finite-element results. Figures 4, 5, and 6 show the absolute value of the errors in the second, fourth, and sixth damping ratios, respectively, and their respective derivative vs the number of modes in the reduced model. The solid line represents the error in the damping ratio, and the dashed lines represent the errors in the updated-mode and the fixed-mode derivatives. Clearly, and not surprisingly, the errors in the derivatives are much larger than the errors in the corresponding damping ratios.

The fixed-mode and updated-mode derivatives were of comparable accuracy. The agreement between the two types of derivatives indicates that the errors associated with the finite-difference calculation of the updated-mode derivatives are small.

The results of damping ratios and their corresponding derivatives for other modes are similar to those presented in that errors in the derivatives are about an order of magnitude larger than the errors in the damping ratios. The comparison of the fixed-mode and the updated-mode derivative indicates that, in the zone where the errors are acceptable, there is no substantial difference between the two methods; thus, the cheaper, fixed-mode method is preferred.

Table 3 Derivatives of first six damping ratios with respect to added mass at two locations (see Fig. 2)

	Derivative, in. · lb^{-1} · s^{-2}	
Mode	Point A	Point B
1	65.72374	20.47085
2	−19.62912	7.540893
3	−34.53779	−34.16656
4	3.3944869	22.11590
5	−31.18742	6.653129
6	55.11845	36.93203

The convergence of the reduced-model derivatives is also a function of the damping in the system. For lower damping, the coupling between the modes decreases and the convergence rate is accelerated. For example, Fig. 7 shows the convergence of the fourth-mode damping ratio and its derivative for gains (c_1 and c_2) that are reduced by one-half. This figure shows that, for a one-half decrease in the damping in the system, the errors in the derivative are reduced by an order of magnitude (compare with Fig. 5).

As in the Fourier example (Fig. 1), we have shown that although the convergence of the damping ratios is good, the convergence of the derivatives of the damping ratios can be poor. However, the modal convergence is misleading when the number of modes approaches the number of degrees of freedom of the finite-element model. When the number of modes is equal to the number of degrees of freedom, the modal and

finite-element analyses are identical. Therefore, the accelerated convergence seen in Figs. 4–6 when the number of modes exceeds 20 may be a consequence of the use of finite-element modes instead of exact modes. To check on this possibility, more refined models were investigated.

Refined Finite-Element Models

To explore the slow convergence of the fourth-mode derivative further, finite-element models with finer meshes, including 6, 9, and 12 beam elements per span (30, 45, and 60 total elements, respectively) were formed. The reduced-model, updated-mode derivatives were calculated, and the errors were referenced to an "exact" derivative value calculated by extrapolating the derivative calculated using the two finest meshes as follows. Reference 9 shows that the error in the finite-element eigenvalues decreases asymptotically with the fourth power of the number of cubic beam elements used in the finite-element model. This can be applied to the derivative of the eigenvalue (thus the derivative of the damping ratio) to give us the relation

$$d_n = d_0 - \alpha n^{-4} \tag{18}$$

where d_n is the finite-element derivative obtained with n elements, d_0 is the exact value of the derivative, and α is a constant. The values d_0 and α were calculated for the fourth-mode derivative using the results of the 45- and 60-element models. The value of d_0 obtained (3.56527 in. $\cdot$ lb^{-1} $\cdot$ s^{-2}) was used as the exact value of the derivative.

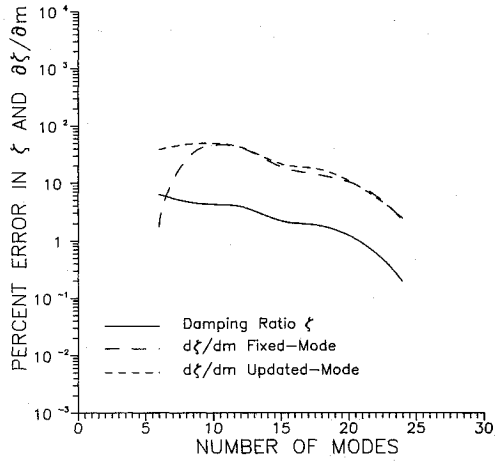

Fig. 7 Convergence of mode 4 damping ratio and derivative with reduced damping.

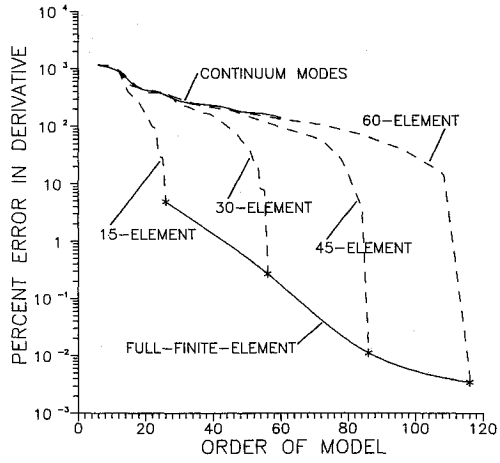

Fig. 8 Convergence of mode 4 derivative: reduced models and finite-element models.

To complete the analogy with the Fourier example, the fourth damping-ratio derivative was also calculated using gradually increasing, reduced-order models based on continuum modes (see the Appendix). As in a Fourier series, the continuum formulation gives us an infinite number of modes to work with. Also, the continuum modes are exact, compared with the approximate modes produced by the finite-element formulations. Again, the errors were calculated with respect to the exact value previously calculated.

We now have three types of models. Two use vibration modes, one with finite-element modes and one with continuum modes, and the third is the full-finite-element model. The order of the model for the first two types is equal to the number of modes, whereas for the third it is equal to the number of finite-element degrees of freedom.

The errors in the derivative of the fourth damping ratio for the three types of models are given in Fig. 8 as a function of the order of the model. The top solid line is the error in the derivative calculated using the continuum modes (see the Appendix). The dashed lines are the errors in the derivative for the four finite-element models using updated modes (and finite differences), and the bottom solid line is the error in the four, full-finite-element derivatives, using Eqs. (10–12).

From Fig. 8 it is clear that the convergence of the continuum, reduced-model derivative is much slower than the finite-element derivative. For the same order, the finite-element derivative is two to four orders of magnitude more accurate. For example, with 26 degrees of freedom, the coarsest finite-element model has an error of about 5%, whereas 26 continuum modes result in an error of about 350%. Clearly, for this problem, the use of vibration modes to reduce the model is counterproductive.

If we follow the convergence of any of the finite-element, reduced-model cases, we see that, for the low-order models, the convergence follows that of the continuum case. This is expected, since the lower modes of a finite-element formulation are quite accurate. But as the higher, *less* accurate modes are added, the rate of convergence *increases*. This is not because the less accurate modes are better at calculating the derivative; it is because, when all of the modes of the finite-element model are included, the result must be the same as for the full-finite-element model. Thus, the reduced-model, finite-element derivatives eventually converge to the full-finite-element value. This produces the paradoxical result that, for a fixed number of modes, the accuracy of the derivative *deteriorates* as the finite-element model is refined. For example, with the coarsest model, 26 modes give the same derivative as the full-finite-element calculation, i.e., an error of 5%. When we use 26 modes with the 30-element model, the derivative is very close to the continuum results; thus, the error increases to about 350%.

Improved Convergence

The slow convergence of the derivative of the Fourier example is associated with the step discontinuity. To show that the slow convergence of the derivative of the damping ratios is associated with the discontinuities introduced by point damping, the structure was reanalyzed with distributed damping. Rotation-rate controllers were used at every node and translation-rate controllers at every node except at the supports. Each type of controller has the same gain.

As before, the gains were designed to produce damping ratios of 1–10% for the first 10 modes. This was accomplished with a translation-rate gain $c_1 = 0.0003$ lb $\cdot$ s $\cdot$ in.$^{-1}$ and rotation-rate gain $c_2 = 0.024$ lb $\cdot$ in. $\cdot$ s. Table 4 shows the full-model (30-element) damping ratios and derivatives of damping ratios with respect to an added mass at point A for the first 10 modes.

Updated-mode derivatives were calculated for gradually increasing size models, and the errors in the damping ratios and derivatives were calculated with respect to the full-finite-element results. Figure 9 show the convergence of the sixth

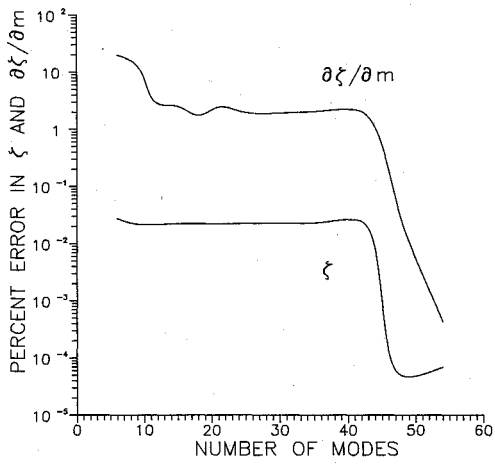

Fig. 9 Convergence of mode 4 damping ratio and derivative with distributed control.

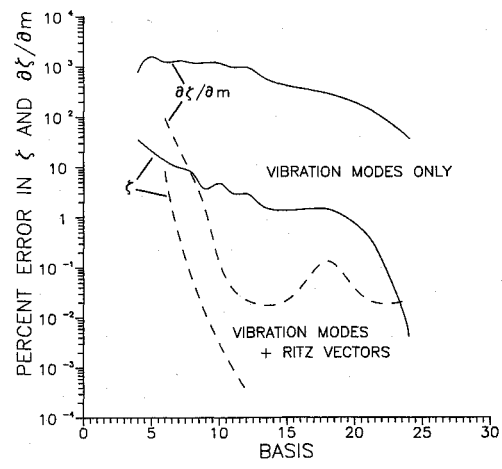

Fig. 10 Convergence comparison of mode 4 damping ratio and derivative: vibration modes only vs vibration modes plus Ritz vectors.

Table 4 Damping ratios and derivatives: distributed damping

Mode	Damping ratio	Derivative
1	0.0879556	−5.49551
2	0.0826721	−3.05576
3	0.0681830	−0.487291
4	0.0558581	−5.28100
5	0.0464619	−3.27698
6	0.0540090	−3.36439
7	0.0532779	−3.38890
8	0.0480473	0.117153
9	0.0433969	−3.37636
10	0.0389295	−3.70461

damping ratio and its derivative (this derivative had the slowest convergence rate of the first six modes).

The damping ratio and derivative converge much faster than that for the point-control case. With the distributed control, the worst-case derivative converges to within 10% error with about 10 modes out of 56 total modes, whereas in the point-control case, it took more than 90% of the available modes to achieve 10% accuracy, regardless of the original size of the finite-element model. Also, the damping ratio is essentially converged for the smallest model.

It has been shown that, when an approximate solution to a dynamic system is obtained using mode superposition, an improved reduced-basis model can be formed by combining the vibration modes with Ritz vectors associated with the static response to the applied loads.[10,11] This accelerated convergence may be caused by the static-response vectors capturing the discontinuities associated with the loading. For the case of a point actuator, it may be similarly advisable to add the static response to point loads at the actuator locations.

Two Ritz vectors corresponding to the static response to a unit load at the translation-rate controller and a unit torque at the rotation-rate controller were added to the eigenvectors to form the reduced model. Thus, for a six-mode model, the two Ritz vectors and the first four vibration modes were used to form the reduced model. The calculations for the reduced-model derivatives were the same as before, except that the reduced mass and stiffness matrices were no longer diagonal.

Figure 10 shows the effect of the additional Ritz vectors on the convergence of the fourth damping ratio and its derivative (the errors are calculated with respect to the full-finite-element results). It can be seen that the convergence is greatly improved with the Ritz vectors for both the damping ratio and derivative. Without the Ritz vectors, there is a 36% error in the derivative with 24 out of 26 modes used. However, with the Ritz vectors included, the derivative converges to within 10% error with only 8 modes.

Since the derivative was taken with respect to a mass located at the displacement-rate controller, it is possible to infer that the desired Ritz vector is associated with the mass rather than with the actuators. To separate the effects of the actuator Ritz vectors and the mass-location Ritz vector, the derivative with respect to an added mass located one-third span to the right of the rotation-rate controller (point B on Fig. 2) was calculated. It was found that the Ritz vectors should be associated with the actuators rather than the point mass.

Concluding Remarks

Modal expansion is a generalization of the Fourier series. It is well known that Fourier series of discontinuous functions converge slowly and that the derivatives of the series may not converge at all. Accordingly, we may expect slow convergence of modal expansion when the applied loads exhibit discontinuities in time or space. In a controlled structure, where most of the damping is supplied by the control system, convergence problems may be caused by point actuators.

A multispan, simply supported beam controlled with a direct-feedback control using point actuators was used to demonstrate that convergence problems due to point actuators do occur. The damping ratios and their derivatives with respect to an added mass were calculated using several finite-element models. Reduced models based on vibration modes were also formed and were used to calculate the damping ratios and their derivatives. Fixed-mode and updated-mode derivative calculation procedures were investigated.

The results showed that errors in the reduced-model derivatives of the damping ratios were about an order of magnitude larger than the errors in the damping ratios themselves. Also, in the zone where the error in the derivatives was acceptable, there was no substantial difference between the fixed-mode derivatives and updated-mode derivatives; thus, the cheaper fixed-mode method is preferred.

To show that the slow convergence of the reduced-model derivatives was due to the point actuators, the beam was analyzed with distributed actuators. In the distributed-actuator case, the derivatives converged much faster.

The convergence of the derivatives with increasing number of modes was compared to the convergence with increasing number of finite-element degrees of freedom. For the derivative of the fourth damping ratio (point-actuator case), it was found that the finite-element approximation converged faster than the modal approximation. This led to a paradoxical situation where improving the accuracy of the modes by using a finer finite-element mesh increased the error of the modal

approximation. This indicates that, in the case of point actuators, it may be impractical to use a modal approximation based solely on vibration modes to calculate derivatives of closed-loop response with respect to structural parameters.

In transient response problems, it is known that complementing the vibration modes with a mode representing static response to the loads can greatly improve convergence. Similarly, for the example studied, it was shown that, if Ritz vectors corresponding to static responses caused by unit loads at the actuators were added to the basis vectors, the convergence of the reduced-model derivatives was greatly enhanced.

Appendix: Continuum Formulation

The equation of motion for the free vibration of a Bernoulli-Euler beam is

$$\frac{d^4V}{dx^4} - \lambda^4 V = 0 \tag{A1}$$

where V is the transverse displacement, x the axial coordinate, and $\lambda^4 = \rho A\omega^2/EI$ (ρ is the mass density, A the cross-sectional area, ω the natural frequency, and EI the bending stiffness). The general solution of Eq. (A1) can be written as

$$V(x) = a\cos\lambda x + b\cosh\lambda x + c\sin\lambda x + d\sinh\lambda x \tag{A2}$$

where $a, b, c,$ and d are constants that depend on the boundary conditions.

Following Ref. 7, we consider a five-span beam, with each span of equal length l (see Fig. 1). If the coordinate system of each span is at the left end of the span, then Eq. (A2) can be written for the rth span as

$$V(x) = a_r\cos\lambda x + b_r\cosh\lambda x + c_r\sin\lambda x + d_r\sinh\lambda x \tag{A3}$$

Since, at $x = 0$, $V = 0$, this reduces to

$$V(x) = a_r(\cos\lambda x - \cosh\lambda x) + c_r\sin\lambda x + d_r\sinh\lambda x \tag{A4}$$

Further conditions that $V = 0$ at all the supports and V' and V'' are continuous at the interior supports give us the following

$$a_r(\cos\lambda l - \cosh\lambda l) + c_r\sin\lambda l + d_r\sinh\lambda l = 0 \tag{A5}$$

$$-a_r(\sin\lambda l + \sinh\lambda l) + c_r\cos\lambda l + d_r\cosh\lambda l = c_{r+1} + d_{r+1} \tag{A6}$$

$$a_r(\cos\lambda l + \cosh\lambda l) + c_r\sin\lambda l - d_r\sinh\lambda l = 2a_{r+1} \tag{A7}$$

Equation (A5) can be written for each span, and Eqs. (A6) and (A7) can be written for each interior support. Since the moment at the left end of the beam is zero, $V''(0) = 0$; thus $a_1 = 0$. The final equation that is needed for the moment at the right end of the beam equal to zero [$V''(l) = 0$].

At this point, we have a 14×14 eigenvalue problem. The eigenvalues are found by solving a transcendental equation developed below. Then the constants are found by dropping one of the eigensystem equations, setting the value of one of the constants equal to one, and then solving for the rest of the constants. In this work, we dropped the last equation [$V''(l) = 0$ in last span] and assumed $c_5 = 1$.

One set of solutions corresponds to $\sin\lambda l = 0$, or

$$\lambda = (n\pi)/l \tag{A8}$$

For the five-span beam, this gives us the eigenvalues for every fifth mode ($\lambda_1, \lambda_6, \ldots$). The mode shapes for these frequencies are just sine functions (a_r, b_r, and c_r are zero). To find the rest of the mode shapes, Eqs. (A5–A7) need to be simplified.

By adding Eq. (A5) to Eq. (A7) and solving for c_r and then subtracting Eq. (A7) from Eq. (A5) and solving for d_r, we get

$$c_r = \frac{a_{r+1} - a_r\cos\lambda l}{\sin\lambda l} \tag{A9}$$

$$d_r = \frac{-a_{r+1} + a_r\cosh\lambda l}{\sinh\lambda l} \tag{A10}$$

as long as $\sin\lambda l \neq 0$. Adding c_r and d_r, we get

$$c_r + d_r = a_r\alpha - a_{r+1}\beta \tag{A11}$$

where $\alpha = \coth\lambda l - \cot\lambda l$ and $\beta = \operatorname{csch}\lambda l - \csc\lambda l$. Similarly, we can show that

$$c_{r+1} + d_{r+1} = a_{r+1}\alpha - a_{r+2}\beta \tag{A12}$$

Equations (A9), (A10), and (A12) can now be substituted into Eq. (A6) and simplified to get

$$a_r\beta - 2a_{r+1}\alpha + a_{r+2}\beta = 0 \tag{A13}$$

This equation can be written for each interior support; thus, for our case we have four equations. As before, a_1 is zero, and since there is no sixth span, a_6 is also zero. We are left with four equations and five unknowns (a_2, a_3, a_4, a_5, and λ). If the determinant of the system is set equal to zero, we get

$$16\alpha^4 - 12\alpha^2\beta^2 + \beta^4 = 0 \tag{A14}$$

This equation can now be solved for the remaining eigenvalues by using a root solver and initial estimates from the finite-element model. Then the 13-equation system can be solved for the mode shapes. Quadruple precision was needed to solve for the higher-frequency mode shapes because the hyperbolic functions made the system singular. The frequencies found from Eq. (A14) fill in the gaps between those given in Eq. (A8).

Once all of the desired frequencies and mode shapes are calculated, generalized system matrices can be generated to calculate damping ratios and their derivatives. This is done by assuming that the damped modes can be approximated by a linear combination of the natural modes above. Using N modes, the damped mode V_r is obtained by solving the eigenvalue problem [Eq. (14)], where $\hat{M}$ and $\hat{K}$ are $N \times N$ diagonal matrices with the generalized masses and stiffnesses on the diagonals. The generalized mass (m_i) and generalized stiffness (k_i) for the ith mode ψ_i are calculated as follows:

$$m_i = \rho A\int_0^l \psi_i^2\,dx \tag{A15}$$

$$k_i = EI\int_0^l (\psi_i'')^2\,dx \tag{A16}$$

Since the integrands are products of trigonometric functions, the integrals can be calculated analytically. The damping matrix for the system is a full matrix calculated as follows:

$$c_{ij} = c_1\psi_i(x_{c_1})\psi_j(x_{c_1}) + c_2\psi_i'(x_{c_2})\psi_j'(x_{c_2}) \tag{A17}$$

where x_{c_1} and x_{c_2} are the location of the controllers. The derivative of the damping ratios were calculated using central finite differences as

$$\frac{\partial\zeta_r}{\partial m} \cong \frac{\zeta_r(\Delta M) - \zeta_r(-\Delta M)}{2\Delta m} \tag{A18}$$

where ΔM is a full $N \times N$ matrix corresponding to the added

mass Δm in generalized coordinates. The elements of ΔM are

$$\Delta M_{ij} = \Delta m \psi_i(x_{\Delta m}) \psi_j(x_{\Delta m}) \quad \text{(A19)}$$

where $x_{\Delta m}$ is the location of the added mass.

Acknowledgment

This work was supported by NASA Grant NAG-1-603.

References

[1]Balas, M. J., "Active Control of Flexible Systems," *Journal of Optimization Theory and Applications*, Vol. 25, July 1978, pp. 415–436.

[2]Czajkowski, E. and Preumont A., "Spillover Stabilization and Decentralized Modal Control of Large Space Structures," *Proceedings of the AIAA Dynamics Specialist Conference*, AIAA, New York, 1987, pp. 599–609.

[3]Onoda, J. and Haftka, R. T., "An Approach to Structure/Control Optimization for Large Space Structures," *AIAA Journal*, Vol. 25, Aug. 1987, pp. 1133–1138.

[4]Haftka, R. T., Martinovic, Z. N., and Hallauer, W. L., Jr., "Enhanced Vibration Controllability by Minor Structural Modification," *AIAA Journal*, Vol. 23, Aug. 1985, pp. 1260–1266.

[5]Haftka, R. T. and Kamat, M. P., *Elements of Structural Optimization*, Nijhoff, Dordrecht, The Netherlands, 1985, pp. 172–173.

[6]Haftka, R. T. and Yates, E. C., Jr., "Repetitive Flutter Calculations in Structural Design," *Journal of Aircraft*, Vol. 13, July 1976, pp. 454–461.

[7]Darnley, E. R., "The Transverse Vibration of Beams and Whirling Shafts Supported at Intermediate Points," *The London, Edinburgh and Dublin Philosophical Magazine and Journal of Science*, Ser. 6, Vol. 41, Jan. 1921, p. 81.

[8]Whetstone, W. D., *EISI-EAL Engineering Analysis Language Reference Guide*, Engineering Information Systems, Inc., San Jose, CA, 1983.

[9]Reddy, J. N., *Applied Functional Analysis and Variational Methods in Engineering*, McGraw-Hill, New York, 1986, p. 401.

[10]Kline, K. A., "Dynamics Analysis Using a Reduced Basis of Exact Modes and Ritz Vectors," *AIAA Journal*, Vol. 24, Dec. 1986, pp. 2022–2029.

[11]Cornwell, R. E., Craig, R. R., Jr., and Johnson, C. P., "On the Application of the Mode-Acceleration Method to Structural Engineering Problems," *Earthquake Engineering and Structural Dynamics*, Vol. 11, Sept.-Oct. 1983, pp. 679–688.